A self-consistent kinetic model for droplet heating and evaporation

S.S. Sazhin[1]*, I.N. Shishkova[2,1], M. Al Qubeissi[1,3]

[1] *Sir Harry Ricardo Laboratories, Centre for Automotive Engineering, School of Computing, Engineering and Mathematics, University of Brighton, Brighton, BN2 4GJ, UK*

[2] *Low Temperature Department, Moscow Power Engineering Institute, Krasnokazarmennaya 14, Moscow 111250, Russia*

[3] *Present address: School of Mechanical, Aerospace and Automotive Engineering, Coventry University, Coventry CV1 2JH, UK*

Abstract

A new kinetic model for heating and evaporation of Diesel fuel droplets is suggested. The model is based on the introduction of the kinetic region in the immediate vicinity of the heated and evaporating droplets, where the dynamics of molecules are described in terms of the Boltzmann equations for vapour components and air, and the hydrodynamic region. The effects of finite thermal conductivity and species diffusivity inside the droplets and inelastic collisions in the kinetic region are taken into account. Diesel fuel is approximated by n-dodecane or a mixture of 80% n-dodecane and 20% p-dipropylbenzene. In both cases, the evaporation coefficient is assumed equal to 1. The values of temperature and vapour density at the outer boundary of the kinetic region are inferred from the requirement that both heat flux and mass flux of vapour (or vapour components) in the kinetic and hydrodynamic regions in the vicinity of the interface between these regions should be equal. Initially, the heat and mass fluxes in the hydrodynamic region are calculated based on the values of temperature and vapour density at the surface of the droplet. Then the values of temperature and vapour density at the outer boundary of the kinetic region, obtained following the above-mentioned procedure, are used to calculate the corrected values of hydrodynamic heat and mass fluxes. The latter in their turn lead to new corrected values of temperature and vapour density at the outer boundary of the kinetic region etc. It is shown that this process quickly converges for the cases analysed in the paper, and it leads to self-consistent values for both heat and mass fluxes. The model is applied to the analysis of heating and evaporation of Diesel fuel droplets with initial radii and temperature equal to 5 μm and 300 K, immersed into gas with temperatures in the range 800-1200 K and pressure equal to 30 bar. It is shown that in all cases the kinetic effects lead to a decrease in droplet surface temperature and an increase in the evaporation time. The kinetic effects on the droplet evaporation time are shown to increase with increasing gas temperatures.

Keywords: Boltzmann equation, Diesel fuel droplet, n-dodecane, p-dipropylbenzene, heat/mass transfer, kinetic effects

Nomenclature

B_M	Spalding mass transfer number
B_T	Spalding heat transfer number
c	specific heat capacity
D	binary diffusion coefficient
E	relative error defined by Equation (13)
F	parameter defined by Equation (9)
h	convection heat transfer coefficient
j	mass flux
k	thermal conductivity
L	latent heat of evaporation
Le	Lewis number
m	mass
Nu	Nusselt number
p	pressure
Pr	Prandtl number
q	heat flux
Q_L	power spent on droplet heating
Re	Reynolds number
R_v	gas constant referring to n-dodecane
R_d	droplet radius
Sc	Schmidt number
Sh	Sherwood number
T	temperature
Y	mass fraction

Greek symbols

α_ρ, α_T	ρ_{Rd}/ρ_s, T_{Rd}/T_s
δ_{Rd}	thickness of the kinetic region
ϵ_i	evaporation rate of individual species
ρ	density
φ	parameter defined by Equation (8)

*Corresponding author: e-mail S.Sazhin@brighton.ac.uk. For data access see http://dx.doi.org/10.17033/DATA.00000009

Subscripts

a	air
cr	critical
d	droplet
e	evaporation
eff	effective
g	gas
h	hydrodynamic
i	components
k	kinetic
mix	mixture
n	n-dodecane
p	constant pressure or p-dipropylbenzene
r	reference
Rd	outer boundary of the kinetic region
s	surface
v	fuel vapour
0	initial
∞	ambient

Superscripts

i	components
sat	saturated
$\sim$	normalised

1. Introduction

In most engineering applications, including automotive ones, the modelling of droplet heating and evaporation processes has been based on the hydrodynamic approximation, when vapour at the droplet surface is assumed to be saturated and the problem of droplet evaporation reduces to the problem of diffusion of vapour from the droplet surface to the ambient gas [1]. At the same time, the limitations of this approximation, even in the case when these processes take place at high pressures, have been well known since

the pioneering papers published more than 100 years ago (see the references in [2]). In a number of studies, including [3]-[8], the evaporation of n-dodecane $C_{12}H_{26}$ (an approximation for Diesel fuel) was studied and a new model combining the kinetic and hydrodynamic approaches was developed. In the immediate vicinity of droplet surfaces (up to about one hundred molecular mean free paths), the vapour and ambient gas dynamics were studied based on the Boltzmann equations for vapour and air (kinetic region), while at larger distances the analysis was based on the hydrodynamic equations (hydrodynamic region). Mass, momentum and energy fluxes were conserved at the interface between these regions. In [9, 10] this approach was generalised to take into account the contribution of two components in liquid and vapour. Using this method, Diesel fuel was approximated as a mixture of n-dodecane (approximating alkanes in Diesel fuel) and p-dipropylbenzene (approximating aromatics in Diesel fuel). The modelling took into account the contributions of three components in the kinetic region (two components approximating Diesel fuel, and air approximated by nitrogen).

In all of the above-mentioned kinetic models it was assumed that the distribution function of evaporated molecules is Maxwellian and vapour pressure at the droplet surface is saturated (mono-component droplets) and obeys Raoult's law (bi-component droplets). The mass flux of evaporated molecules was controlled by the evaporation coefficient, which is the ratio of the actual mass flux of molecules leaving the droplet surface and the maximal possible one. In the earliest publication [3] this coefficient was assumed to be equal to 0.04 and 0.5 (minimal and average values of this coefficient for water). Later, it was assumed equal to 1, except in [8]. In the analysis presented in [8] the values of this coefficient inferred from molecular dynamic simulations of the evaporation of n-dodecane [11] were used. The analysis presented in [11] was based on the so called Force Field (FF) approximation, when quantum mechanics effects due to the contribution of electron shells were not taken into account. Later it was shown that quantum mechanics effects do not have significant influence on the values of this coefficient [12, 13]. As shown in our previous papers (e.g. [8]) the effect of the evaporation coefficient on the droplet evaporation rate is relatively small. In our analysis this coefficient is assumed to be equal to 1.

In all models described in [3]-[8] and [10] the boundary condition at the interface between the kinetic and hydrodynamic regions was inferred based on the requirement of the conservation of heat and mass fluxes at this interface. The hydrodynamic heat and mass fluxes were calculated based on the simplifying assumptions that the temperature at the outer boundary of the kinetic region is equal to the droplet surface temperature and vapour pressure at this boundary is equal to the saturated vapour pressure at temperature equal to the droplet surface temperature. The requirement of the conservation of heat and mass fluxes at this interface allowed the authors of the models described in [6]-[8] and [10] to find the corrected values of temperature and vapour density. The main problem with this approach is that the heat and mass fluxes in the hydrodynamic region, calculated based on these corrected values of temperature and vapour density, are not equal to the heat and mass fluxes in the hydrodynamic region used to find these corrected values,

in the general case. The only feasible way to overcome this problem seems to be to perform iterations; that is, to use the corrected values of temperature and vapour density (or densities in the case of bi-component droplets) at the outer boundary of the kinetic region to calculate the corrected values of hydrodynamic heat and mass fluxes. The latter in their turn would lead to new corrected values of temperature and vapour density at the outer boundary of the kinetic region etc. If this process converges then we would expect to obtain self-consistent values for both heat and mass fluxes. The main objective of this paper is to present the results of the development of the new kinetic model, based on the above-mentioned iteration process, leading to the discovery of self-consistent heat and mass fluxes, and the application of this model to the analysis of droplet heating and evaporation in realistic Diesel engine-like conditions.

The mathematical models, used in the analysis of the processes in the hydrodynamic and kinetic regions, are briefly summarised in Section 2. The iteration processes used in our analysis and the results of their application are described in Section 3 for conditions typical of Diesel engines in the cases where Diesel fuel is approximated by n-dodecane and a mixture of n-dodecane and p-dipropylbenzene. The results of applications of the new model to the analysis of Diesel fuel droplet heating and evaporation in typical Diesel engine-like conditions are presented in Section 4. The main results of the paper are summarised in Section 5.

2. Mathematical models

As in most of our previous papers (e.g. [10]), two regions above the surface of an evaporating fuel droplet, the kinetic and hydrodynamic regions, are considered. We take into account the fact that the thermal conductivity of the liquid phase is finite, and identify the third region as the liquid phase region. All three regions are schematically shown in Fig. 1. T_s and $\rho_{s\,(n,p)}$ refer to the surface temperature and vapour density of n-dodecane (n) and p-dipropylbenzene (p) in the immediate vicinity of the droplet surface; T_{Rd} and $\rho_{Rd\,(n,p)}$ refer to the same parameters but at the interface between the kinetic and the hydrodynamic regions. δ_{Rd} is the thickness of the kinetic region. As in [10], we take into account the diffusion of species in the liquid phase and the presence of up to 3 components in the kinetic region. The conventional hydrodynamic analysis is applied in the liquid and hydrodynamic regions, while vapour and air dynamics in the kinetic region are described by the Boltzmann equations.

The mathematical models for all three regions, used in our analysis, are essentially the same as described in [14, 10]. In what follows the most essential features of these models are briefly summarised.

As in [14, 10], the effects of finite thermal conductivity and species diffusivity in the liquid phase are taken into account based on the analytical solutions to the heat conduction and species diffusion equations inside droplets, assuming that all processes are spherically symmetric. Both solutions are generalised to the case of moving droplets using the effective thermal conductivity and effective diffusivity models. Raoult's

law for the partial pressures of vapour species at the surface of the droplets is assumed to be valid in the case of bi-component droplets. The effects of the curvature of the droplet surface are ignored.

A system of up to three Boltzmann equations (for up to two vapour species, and air approximated by nitrogen) is solved in the kinetic region, assuming that the evaporation coefficient for all species is equal to 1. The effects of both elastic and inelastic collisions are taken into account, using the same approach as in [10]. The boundary conditions at the interface between the kinetic and hydrodynamic regions are formulated as:

$$j_{k\ (n,p)} = j_{h\ (n,p)} \tag{1}$$

(mass flux leaving the kinetic region (k) is equal to the mass flux entering the hydrodynamic region (h) for n-dodecane (n) and p-dipropylbenzene (p)) and

$$q_k = q_h \tag{2}$$

(heat flux leaving the kinetic region (k) is equal to the heat flux entering the hydrodynamic region (h)).

The values of $j_{k\ (n,p)}$ and q_k were calculated based on the solution to Boltzmann equations, while $j_{h\ (n,p)}$ and q_h in the hydrodynamic region were estimated as [14, 10]:

$$j_{h\ (n,p)} = -\frac{\epsilon_i \dot{m}_d}{4\pi R_d^2} = \frac{D_v \rho_{\text{total}}}{2R_d} \epsilon_i \text{Sh}^* \ln(1 + B_M), \tag{3}$$

(i refers either to n-dodecane ($i = n$) or p-dipropylbenzene ($i = p$)) and

$$q_h = \frac{k_{\text{mix}}}{R_d} \text{Nu}^* \frac{\ln(1 + B_T)}{2B_T} (T_g - T_{Rd}) = h(T_g - T_{Rd}), \tag{4}$$

where

$$\epsilon_i = \frac{Y_{viRd}}{\sum_{i=n,p} Y_{viRd}}, \tag{5}$$

the subscripts $_v$ and $_{Rd}$ indicate the vapour phase and the interface between the kinetic and hydrodynamic regions respectively, Y_v is the vapour mass fraction,

$$B_M = \frac{\rho_{vRd} - \rho_{v\infty}}{\rho_{gRd}} = \frac{Y_{vRd} - Y_{v\infty}}{1 - Y_{vRd}}, \tag{6}$$

$B_T = \frac{c_{pv}(T_g - T_s)}{L_{\text{eff}}}$, $L_{\text{eff}} = L + \frac{Q_L}{\dot{m}_d} = \sum_i \epsilon_i L_i + \frac{Q_L}{\sum_i \dot{m}_i}$, Q_L is the power spent on droplet heating, c_{pv} is the specific heat capacity of fuel vapour (estimated for the mixture of vapour species in the case of bi-component droplets), B_T and B_M are linked by the equation

$$B_T = (1 + B_M)^{\varphi} - 1, \tag{7}$$

$$\varphi = \left(\frac{c_{pv}}{c_{pa}}\right) \left(\frac{\text{Sh}^*}{\text{Nu}^*}\right) \frac{1}{\text{Le}}, \tag{8}$$

$\text{Le} = k_a/(c_{pa}\rho_{\text{total}} D_v) = \text{Sc}_d/\text{Pr}_d$ is the Lewis number,

$$\text{Sh}^* = 2\left(1 + \frac{(1 + \text{Re}_d \text{Sc}_d)^{1/3} \max\left[1, \text{Re}_d^{0.077}\right] - 1}{2F(B_M)}\right),$$

$$\mathrm{Nu}^* = 2\left(1 + \frac{\left(1 + \mathrm{Re}_d \mathrm{Pr}_d\right)^{1/3} \max\left[1, \mathrm{Re}_d^{0.077}\right] - 1}{2F(B_T)}\right),$$

$$F(B_{T,M}) = (1 + B_{T,M})^{0.7} \frac{\ln(1 + B_{T,M})}{B_{T,M}}, \tag{9}$$

Re_d, Pr_d, Sc_d are Reynolds (based on droplet diameter), Prandtl, and Schmidt numbers respectively, h is the convection heat transfer coefficient. As in the analysis presented in our previous papers (e.g. [10]), we assume that the mass diffusion coefficients in the gas phase for both components (D_v) are the same.

The vapour saturated pressures and other thermodynamic parameters and transport coefficients for liquid and vapour for n-dodecane and p-dipropylbenzene are taken to be the same as in [10] (for n-dodecane these values were ultimately taken from [15]). Thermodynamic and transport properties of the mixture of vapour and air are assumed to be the same as those of pure air (vapour is assumed to be diluted). For example the thermal conductivity of the mixture k_{mix} in Expression (4) is assumed to be equal to that of air. All air properties are taken from [16]. To find the temperature and vapour density at the outer boundary of the kinetic region, Expression (8) was simplified to:

$$\varphi = \left(\frac{c_{pv}}{c_{pa}}\right) \frac{1}{\mathrm{Le}}, \tag{10}$$

assuming that $\mathrm{Sh}^*/\mathrm{Nu}^*$ is close to 1 (this allowed us to avoid an additional iteration loop on top of the one described in the next section). The general Expression (8) was used in the hydrodynamic calculations, the results of which, in their turn, were used as input parameters in the kinetic model. Equation (10) is strictly valid in the case of stationary droplets only. The validity of this approximation for moving droplets in typical Diesel engine conditions was demonstrated in [17].

All liquid properties are calculated for the average temperature inside droplets. All gas properties are calculated for the reference temperature $T_r = (2/3)T_s + (1/3)T_g$, where T_s and T_g are droplet surface and ambient gas temperature respectively. Enthalpy of evaporation and saturated vapour pressure are estimated at the surface temperature T_s.

Note that the expressions for saturated vapour pressure (p^{sat}) for n-dodecane and p-dipropylbenzene used in our analysis cannot be considered reliable at temperatures close to or above the critical temperatures. Heating and evaporation of the droplets at these temperatures, sometimes predicted by the model at the very final stage of droplet evaporation, does not describe accurately the physical background of the processes at this stage. The contribution of the processes at this stage to the overall droplet heating and evaporation, however, is expected to be small. To mitigate this behaviour of droplet surface temperature, the saturated pressures were artificially increased when the temperatures approached or exceeded the corresponding critical temperatures, using the following formula:

$$p^{\mathrm{sat\ (corrected)}} = \begin{cases} p^{\mathrm{sat}} & \text{when} \quad T \le 0.99\,T_{\mathrm{cr}} \\ \exp\left[15(T - 0.99\,T_{\mathrm{cr}})/0.99\,T_{\mathrm{cr}}\right] p^{\mathrm{sat}} & \text{when} \quad T > 0.99\,T_{\mathrm{cr}}, \end{cases} \tag{11}$$

where $_{\rm cr}$ indicates the critical temperature. This correction affected the very final stage of droplet evaporation (when their mass becomes less than about 1% of the initial mass in most cases) and produced negligible effects on the overall process of droplet heating and evaporation.

Since the values of fuel vapour density and temperature at level $_{Rd}$ (outer boundary of the kinetic region) are not known, at the first step these values are assumed equal to those at the droplet surface (level $_s$).

As in [10], the first step in the solution of the Boltzmann equations was to perform an investigation into mass and heat transfer processes in the kinetic region for a set of values of ρ_{Rd} (for each of the vapour components separately in the case of bi-component droplets) and T_{Rd}. These parameters were assumed to be in the ranges: $\rho_{Rd} < \rho_s$ and $T_{Rd} > T_s$ (heating of droplets in a hot gas). For the chosen values of ρ_{Rd} and T_{Rd}, the solution to the Boltzmann equations in the kinetic region allowed us to calculate the normalised mass and heat fluxes at the outer boundary of this region:

$$\tilde{j}_{\rm k\,(n,p)} \equiv j_{\rm k\,(n,p)}/(\rho_0\sqrt{R_v T_0}), \qquad \tilde{q}_{\rm k} \equiv q_{\rm k}/(p_0\sqrt{R_v T_0}),$$

where R_v is the gas constant referring to n-dodecane vapour, T_0 is the reference temperature chosen equal to 600 K, p_0 and ρ_0 are the saturated n-dodecane vapour pressure and density corresponding to T_0, ρ_0 was calculated from the ideal gas law. In [8, 10] it was shown that for the case of heating and evaporation of n-dodecane or a mixture of n-dodecane and p-dipropylbenzene droplets, the values of $\tilde{q}_{\rm k}$ are almost independent of $\alpha_\rho \equiv \rho_{Rd}/\rho_s$ in a certain range of α_ρ and the values of $\tilde{j}_{\rm k}$ are almost independent of $\alpha_T \equiv T_{Rd}/T_s$ in a certain range of α_T relevant to the conditions typical for Diesel engines.

At the same time for both mono- and bi-component droplets it was shown that $\tilde{q}_{\rm k}$ increases almost linearly with increasing α_T, and $\tilde{j}_{\rm k}$ decreases almost linearly with increasing α_ρ. As mentioned earlier, in our previous papers the values of T_{Rd} and ρ_{Rd} were found from Equations (1) and (2), assuming that $\alpha_T = 1$ and $\alpha_\rho = 1$ for the hydrodynamic model. A more accurate model for finding these parameters, focused on the calculation of self-consistent fluxes, is described in the next section.

3. Calculation of self-consistent mass and heat fluxes

Let us assume that Diesel fuel can be approximated by n-dodecane, a droplet is stationary and its surface temperature is equal to 600 K; gas temperature and pressure are assumed equal to 1000 K and 30 bar respectively. The plots of $\tilde{j}_{\rm k} \equiv j_{\rm k\,n}/(\rho_0\sqrt{R_v T_0})$ versus α_ρ and $\tilde{q}_{\rm k} \equiv q_{\rm k}/(p_0\sqrt{R_v T_0})$ versus α_T are shown in Figs. 2 and 3 respectively (lines indicated as 'k'). In the same figures, the plots of $\tilde{j}_{\rm h} \equiv j_{\rm h\,n}/(\rho_0\sqrt{R_v T_0})$ versus α_ρ and $\tilde{q}_{\rm h} \equiv q_{\rm h}/(p_0\sqrt{R_v T_0})$ versus α_T, assuming that $\alpha_\rho = 1$ and $\alpha_T = 1$, are also shown (lines marked 'h', iteration 1). The intersection between these two pairs of lines gave the values $\alpha_\rho = 0.994$ and $\alpha_T = 1.036$. In our previous analysis these corrections were directly used for calculation of mass and heat fluxes, taking into account the kinetic effects. In the new model, these corrections are used for updating the

values of $\tilde{j}_{\rm h}$ and $\tilde{q}_{\rm h}$, and the updated values of these fluxes are shown in Figs. 2 and 3 as the lines marked 'h', iteration 2. The intersections of these new lines with lines $\tilde{j}_{\rm k}$ and $\tilde{q}_{\rm k}$ provide us updated values $\alpha_\rho = 0.993$ and $\alpha_T = 1.034$. Further iterations up to iteration 50 do not lead to any visible changes in these corrections, as shown in the same Figs. 2 and 3. As follows from the above analysis, the calculation of self-consistent fluxes leads to a slight decrease in the values of both α_ρ and α_T for a droplet surface temperature of 600 K. Note that, in contrast to the previously used non-self-consistent model, our new approach does not rely on the observation that $\tilde{q}_{\rm k}$ is almost independent of α_ρ and $\tilde{j}_{\rm k}$ is almost independent of α_T.

The same iteration procedure and for the same conditions as presented in Figs. 2 and 3, but for droplets moving with relative velocity equal to 10 m/s, is shown in Figs. 4 and 5. Comparing the plots shown in Figs. 2 and 3 with those shown in Figs. 4 and 5, one can see that in the case of the moving droplets there is a visible difference between the values of α_ρ and α_T predicted after the second and 50th iterations. The difference in the values of α_ρ and α_T inferred from consecutive iterations decreases with increasing iteration number, so that the differences between these values inferred from the 49th iteration are almost indistinguishable from those inferred from the 50th iteration. The values of α_ρ and α_T for the self-consistent mass and heat fluxes predicted for the moving droplet are visibly lower than the ones predicted for the stationary droplet.

The same analysis as presented in Figs. 2-5 was repeated for other droplet surface temperatures in the range 300-650 K and gas temperatures 800 K, 1000 K and 1200 K. Also, the same analysis was repeated for bi-component droplets (80% n-dodecane and 20% p-dipropylbenzene mixture) for droplet surface temperatures in the range 300-650 K and gas temperature equal to 1000 K. The predictions of the kinetic model at temperatures close to the critical temperature of n-dodecane ($T_{\rm cr} = 659$ K) proved to be unreliable and it was assumed that the values of α_ρ and α_T at $T_s > 650$ K are the same as at $T_s = 650$ K. This assumption is expected to affect the very final stage of droplet evaporation, and has limited effect on the overall picture of droplet heating and evaporation. As mentioned in our earlier paper [10], both hydrodynamic and kinetic models are not reliable at high gas temperature. For example, the derivation of Expression (3) was based on the assumption that $\rho_{\rm total}$ does not depend on the distance from the droplet surface. This cannot be satisfied in the case of large differences between the values of droplet surface and gas temperatures. The model in which this assumption is relaxed was suggested in [18, 19], but it is too complex for use in our analysis, and is based on several additional assumptions the applicability of which to Diesel engine-like conditions is not at first evident.

The results of the above-mentioned analyses are presented in the form of the plots of α_ρ and α_T versus droplet surface temperatures T_s for various gas temperatures and droplet velocities and compositions, shown in Figs. 6-19. Ambient gas pressure in all cases is equal to 30 bar. The plots shown in Figs. 6 and 7 refer to stationary n-dodecane droplets immersed into gas at temperature 800 K. As can be seen from Fig. 6, the values of α_ρ decrease with increasing T_s. The values of α_ρ inferred from iteration 2 are slightly lower than those inferred from iteration 1, and are almost indistinguishable from those inferred from all the following

iterations up to iteration 50. The behaviour of the curve α_T versus T_s, shown in Fig. 7, appears to be more complex than that of α_ρ versus T_s. For low temperatures α_T increases with increasing T_s, at intermediate temperatures α_T decreases with increasing T_s, and at temperatures close to 650 K, α_T again increases with increasing T_s. As in the case of α_ρ, the values of α_T inferred from iteration 2 and higher iterations are almost indistinguishable. These values are slightly higher than those inferred from iteration 1 for low T_s and slightly lower than those inferred from iteration 1 for high T_s. In our analysis, the values inferred from iteration 50 are assumed to describe adequately the self-consistent heat and mass fluxes in the vicinity of the surfaces of heated and evaporating droplets.

The same plots as presented in Figs. 6 and 7, but for gas temperature equal to 1000 K, are shown in Figs. 8 and 9. The curves shown in Figs. 8 and 9 are similar to those shown in Figs. 6 and 7, except that the difference between the values of α_ρ and α_T inferred from iterations 2-50 and those inferred from iteration 1, are larger in the case of gas temperature equal to 1000 K than in the case of gas temperature equal to 800 K. The values of these coefficients at $T_s = 600$ K are the same as shown in Figs. 2 and 3.

The same plots as presented in Figs. 8 and 9, but for droplets moving with velocity 10 m/s, are shown in Figs. 10 and 11. The general shapes of the curves shown in Figs. 10 and 11 are similar to those shown in Figs. 8 and 9, although comparing these curves one can see that droplet movement leads to increased difference between the values of α_ρ and α_T, inferred from iterations 1 and 2 (and all the following iterations). As can be seen from Fig. 10, the values of α_ρ inferred from iteration 3 are almost indistinguishable from those inferred from iteration 50. This pattern was observed for all other curves although in most cases this is not explicitly demonstrated.

The same plots as presented in Figs. 8 and 9, but for gas temperature equal to 1200 K, are shown in Figs. 12 and 13. The curves shown in Figs. 12 and 13 are similar to those shown in Figs. 8 and 9, except that the values of α_ρ tend to be lower and the values of α_T tend to be higher for gas temperature 1200 K compared with the case of gas temperature 1000 K. This shows a tendency for enhanced kinetic effects with increasing gas temperature.

Let us now consider the case when Diesel fuel is approximated by a mixture of 80% n-dodecane and 20% p-dipropylbenzene and gas temperature and pressure are equal to 1000 K and 30 bar respectively. Droplets are assumed to be stationary. The plots of $\alpha_{\rho\, n} \equiv \rho_{Rd\,(n)}/\rho_{s\,(n)}$ (normalised n-dodecane density) versus T_s, calculated following the procedure shown in Figs. 2 and 4 and inferred from iterations 1-50, are presented in Fig. 14. The results inferred from iteration 2 and all the following iterations turned out to be indistinguishable. Comparing Figs. 14 and 8 one can see that the presence of the second component does not affect the trends of the curves $\alpha_{\rho\, n}$ versus T_s.

The same plots as shown in Fig. 14 but for $\alpha_{\rho\, p} \equiv \rho_{Rd\,(p)}/\rho_{s\,(p)}$ (normalised p-dipropylbenzene density) versus T_s are presented in Fig. 15. Comparing Figs. 15 and 14 one can see that the values of $\alpha_{\rho\, p}$ are visibly larger than the values of $\alpha_{\rho\, n}$ (kinetic effects for p-dipropylbenzene are weaker than for n-dodecane).

The plots of $\alpha_T \equiv T_{Rd}/T_s$ (normalised temperature at the outer boundary of the kinetic region) versus T_s, calculated following the procedure shown in Figs. 3 and 5 and inferred from iterations 1-50, are presented in Fig. 16. The general shapes of the curves shown in this figure are similar to those shown in Figs. 7, 9, 11 and 13. The results for iteration 2 are almost indistinguishable from those for iteration 3 and all the following iterations up to iteration 50.

The same plots as presented in Figs. 14 and 15, but for a droplet moving with velocity 10 m/s, are shown in Figs. 17 and 18. Comparing the plots shown in Figs. 14 and 15 and those shown in Figs. 17 and 18, one can see that the movement of droplets leads to increased deviation between the values of coefficients inferred from iteration 1 and the following iterations.

The same plots as presented in Fig. 16, but for the droplet moving with velocity 10 m/s, are shown in Fig. 19. Comparing the plots shown in Fig. 16 and those shown in Fig. 19, one can see that the movement of droplets leads to increased deviation between the values of coefficients inferred from iteration 1 and the following iterations. The values of $\alpha_{\rho\, n}$ and $\alpha_{\rho\, p}$ tend to be smaller and the values of α_T tend to be larger for moving droplets compared with stationary ones.

The values of α_ρ ($\alpha_{\rho\, n}$ and $\alpha_{\rho\, p}$ in the case of bi-component droplets) and α_T shown in Figs. 6-19 were used to modify equations for the hydrodynamic model to take into account the kinetic effects. In the case of mono-component droplets, the corrections α_ρ lead to the replacement of Y_s with $Y_{Rd} = \alpha_\rho Y_s$ and the corresponding modifications of Spalding numbers B_M and B_T (see Equations (6) and (7)). The modification of B_M leads to the corresponding modification of the mass flux from the surface of the evaporating droplets (see Equation (3)). Also, the corrections α_T lead to the replacement of T_s with $T_{Rd} = \alpha_T T_s$. The modifications of B_T and T_s lead to the modification of the heat flux reaching heated and evaporating droplets described by Equation (4).

In the case of multi-component (bi-component in the case studied in our paper) droplets, the corrections $\alpha_{\rho\, n}$ lead to the replacement of $Y_{s\,(n)}$ with $Y_{Rd\,(n)} = \alpha_{\rho\, n} Y_{s\,(n)}$, and the corrections $\alpha_{\rho\, p}$ lead to the replacement of $Y_{s\,(p)}$ with $Y_{Rd\,(p)} = \alpha_{\rho\, p} Y_{s\,(p)}$. The value of Y_{Rd} in this case is calculated as $Y_{Rd\,(n)} + Y_{Rd\,(p)}$. Similarly the value of ϵ_i is modified to take into account the kinetic effects, using the definition of this parameter (see Equation (5)). The remaining analysis is the same as in the case of the mono-component droplet.

To take into account the kinetic effects in the analytical solution for the temperature inside droplets we make the following replacement:

$$h \rightarrow h^k = h(B_T^k)\frac{T_g - T_{Rd}}{T_g - T_s} \tag{12}$$

In our analysis, the values of α_ρ ($\alpha_{\rho\, n}$ and $\alpha_{\rho\, p}$ in the case of bi-component droplets) and α_T shown in Figs. 6-19 were approximated by analytical formulae shown in Appendix 1. Unfortunately, these analytical formulae were derived for a limited set of gas temperatures and this limits their potential for implementation

in Computational Fluid Dynamics (CFD) codes, to take into account kinetic effects, without first performing proper kinetic calculations. Once these analytical formulae are obtained for more gas temperatures relevant to Diesel engine applications, similar analytical expressions describing the effects of gas temperatures on the values of α_ρ ($\alpha_{\rho\, n}$ and $\alpha_{\rho\, p}$ in the case of bi-component droplets) and α_T could potentially be obtained. This approach could possibly be more efficient for approximating kinetic results compared with the direct comparison between the values of droplet radii and surface temperatures predicted by hydrodynamic and kinetic models as suggested in [20]). The feasibility of this approach for a wide range of parameters has yet to be investigated.

In the next section, the results of modelling of Diesel fuel droplet heating and evaporation, using the model described above, are demonstrated.

4. Droplet heating and evaporation

The results of calculation of the radii and surface temperatures versus time for a stationary n-dodecane droplet with initial radius and temperature equal to 5 μm and 300 K respectively, immersed into gas with temperature 1000 K and pressure 30 bar, predicted by the hydrodynamic and kinetic models described in the previous section (for iteration 50), are shown in Fig. 20. As one can see from this figure, the kinetic effects lead to a slight reduction of the droplet surface temperature and a noticeable increase in the evaporation time. This increase is described by parameter E_k, defined as

$$E_k = \frac{t_{e\,k} - t_{e\,h}}{t_{e\,k}} \times 100\%, \tag{13}$$

where $t_{e\,k}$ and $t_{e\,h}$ are droplet evaporation times predicted by the kinetic and hydrodynamic models respectively. In the case of the plots shown in Fig. 20, $E_k = 3.7\%$.

It was shown that the decrease/increase in gas temperature leads to an increase/decrease in the evaporation time as expected. Comparing the calculations for gas temperatures 800 K, 1000 K and 1200 K, and droplet velocities 0 and 10 m/s we were able to show that for mono-component droplets the relative increase in the evaporation times due to kinetic effects is more visible at high gas temperatures and droplet velocities. For stationary droplets the values of E_k increased from 3.2% to 5.0% when gas temperature increased from 800 K to 1200 K. For droplets moving with a velocity of 10 m/s the values of E_k were found to be 5.7%, 6.7% and 6.4% for gas temperatures 800 K, 1000 K and 1200 K, respectively. For all gas temperatures and droplet velocities under consideration, the kinetic effects led to a slight reduction in the droplet surface temperature.

The same plots as shown in Fig. 20, but for a bi-component droplet (a mixture of 80% n-dodecane and 20% p-dipropylbenzene) are presented in Fig. 21. Comparing the curves shown in Figs. 20 and 21, one can see that the addition of p-dipropylbenzene leads to a slight increase in the droplet evaporation time, without noticeable changes in other properties. In this case, $E_k = 2.8\%$.

The same plots as shown in Fig. 20, but for a bi-component droplet moving with velocity 10 m/s, are presented in Fig. 22. As in the case of stationary droplets, one can see that the addition of p-dipropylbenzene leads to a slight increase in the droplet evaporation time, without noticeable changes in other properties. In this case, $E_k = 5.7\%$.

The plots of mass fractions of n-dodecane ($Y_{s\,n}$) and p-dipropylbenzene ($Y_{s\,p}$) at the surface of the droplet, predicted by hydrodynamic and kinetic models, versus time for the same droplet as described in Fig. 22 are shown in Fig. 23. As one can see from this figure, at the final stage of droplet evaporation the mass fraction of n-dodecane decreases (this is the most volatile component in the mixture) and the mass fraction of p-dipropylbenzene increases (this is the least volatile component in the mixture). This explains why the addition of p-dipropylbenzene leads to an increase in the droplet evaporation time.

Note that the analysis so far has been focused on droplets with initial radii 5 μm. The kinetic effects decrease with increasing droplet radii (e.g. [20]). For smaller droplet radii, the kinetic effects are expected to be more pronounced compared with those for droplets with radii equal to 5 μm. The contribution of these droplets in Diesel engines, however, is expected to be small. Also, the analysis of the kinetic effects for these small droplets would require taking into account the effects of surface tension on the heat transfer and evaporation processes (these were ignored in our analysis).

Comparing the plots shown above and the corresponding plots predicted by the non-self-consistent model, described in our previous paper [10], one can see that in most cases the self-consistent model leads to larger kinetic corrections compared with those predicted by the non-self-consistent model for the cases considered in our paper.

5. Conclusions

A new kinetic model for heating and evaporation of droplets is suggested and applied to the analysis of Diesel fuel droplet heating and evaporation in Diesel engine-like conditions. As in our previous papers (e.g. [8, 10]), the model is based on the introduction of the kinetic region in the immediate vicinity of the heated and evaporating droplets, where the dynamics of molecules are described in terms of the Boltzmann equations for vapour components and air, and the hydrodynamic region. The boundary conditions at the outer boundary of the kinetic region are introduced by matching the heat fluxes and mass fluxes of vapour components leaving the kinetic region and entering into the surrounding hydrodynamic region. The effects of finite thermal conductivity and species diffusivity inside the droplets and inelastic collisions in the kinetic region are taken into account. Diesel fuel is approximated by n-dodecane or a mixture of 80% n-dodecane and 20% p-dipropylbenzene. In both cases, the evaporation coefficient is assumed equal to 1.

Attention is drawn to the fact that in the previous papers (e.g. [8, 10]) the heat and mass fluxes in the hydrodynamic region, based on which the temperature and vapour density at the outer boundary of the

kinetic region were obtained, were calculated based on the values of temperature and vapour density at the surface of the droplet. These values are not the same as those at the outer boundary of the kinetic region, and this means that the whole approach used in [8, 10] is not self-consistent.

To overcome this problem iterations were used. The values of temperature and vapour density at the outer boundary of the kinetic region, obtained following the above-mentioned procedure, were used to calculate the corrected values of hydrodynamic heat and mass fluxes. The latter in their turn led to new corrected values of temperature and vapour density at the outer boundary of the kinetic region etc. It was shown that this process quickly converges for the cases analysed in the paper, and it leads to self-consistent values for both heat and mass fluxes.

Following this procedure, a set of coefficients $\alpha_\rho \equiv \rho_{Rd}/\rho_s$ (normalised vapour density at the outer boundary of the kinetic region) and $\alpha_T \equiv T_{Rd}/T_s$ (normalised temperature at the outer boundary of the kinetic region) were obtained for a set of conditions and droplet surface temperatures in the range 300-650 K, assuming that Diesel fuel can be approximated by n-dodecane. In the case when Diesel fuel was approximated by a mixture of n-dodecane and p-dipropylbenzene, α_ρ was replaced with $\alpha_{\rho\, n} \equiv \rho_{Rd\ (n)}/\rho_{s\ (n)}$ (normalised n-dodecane density) and $\alpha_{\rho\, p} \equiv \rho_{Rd\ (p)}/\rho_{s\ (p)}$ (normalised p-dipropylbenzene density). These coefficients were implemented into the hydrodynamic code and used for calculation of Diesel fuel droplet heating and evaporation.

The model was applied for the analysis of heating and evaporation of Diesel fuel droplets with initial radii and temperature equal to 5 μm and 300 K, immersed into gas with temperatures equal to 800 K, 1000 K and 1200 K and pressure equal to 30 bar. Droplets were stationary or moving with velocity equal to 10 m/s. It was shown that in all cases the kinetic effects led to a decrease in droplet surface temperature and an increase in the evaporation time. This increase is shown to be more visible for higher gas temperatures and moving droplets. The addition of p-dipropylbenzene is shown to decrease the kinetic effects on the droplet evaporation time.

Acknowledgments

The authors are grateful to EPSRC (UK) (Project EP/J006793/1), INTERREG IVa (Project E3C3, Reference 4274) and the Russian Foundation for Basic Research (Grant 14-08-00467) for their financial support of this project.

References

[1] S.S. Sazhin, Droplets and Sprays. Springer (2014).

[2] N.A. Fuchs, Evaporation and Droplet Growth in Gaseous Media. London: Pergamon Press (1959).

[3] A.P. Kryukov, V.Yu. Levashov, S.S. Sazhin, Evaporation of Diesel fuel droplets: kinetic versus hydrodynamic models, Int. J. Heat Mass Transfer 47 (2004) 2541-2549.

[4] I.N. Shishkova, S.S. Sazhin, A numerical algorithm for kinetic modelling of evaporation processes, J. Computational Physics 218 (2006) 635-653.

[5] S.S. Sazhin, I.N. Shishkova, A.P. Kryukov, V.Yu. Levashov, M.R. Heikal, Evaporation of droplets into a background gas: kinetic modelling, Int. J. Heat Mass Transfer 50 (2007) 2675-2691.

[6] S.S. Sazhin, I.N. Shishkova, A kinetic algorithm for modelling the droplet evaporation process in the presence of heat flux and background gas, Atomization and Sprays 19 (2009) 473-489.

[7] I.N. Shishkova, S.S. Sazhin, J.-F. Xie, A solution of the Boltzmann equation in the presence of inelastic collisions, J. Computational Physics 232 (2013) 87-99.

[8] S.S. Sazhin, J.-F Xie, I.N. Shishkova, A.E. Elwardany, M.R. Heikal, A kinetic model of droplet heating and evaporation: effects of inelastic collisions and a non-unity evaporation coefficient, Int. J. Heat and Mass Transfer 56 (2013) 525-537.

[9] I.N. Shishkova, S.S. Sazhin, A solution of the Boltzmann equation in the presence of three components and inelastic collisions, Int. J. Heat and Mass Transfer 71 (2014) 26-34.

[10] S.S. Sazhin, I.N. Shishkova, M. Al Qubeissi, Heating and evaporation of a two-component droplet: Hydrodynamic and kinetic models, Int. J. Heat and Mass Transfer 79 (2014) 704-712.

[11] J.-F. Xie, S.S. Sazhin, B.-Y. Cao, Molecular dynamics study of the processes in the vicinity of the n-dodecane vapour/liquid interface, Phys. Fluids 23 (2011) 112104.

[12] V.M. Gun'ko, R. Nasiri, S.S. Sazhin, Effects of the surroundings and conformerisation of n-dodecane molecules on evaporation/condensation processes, J Chemical Physics 142 (2015) 034502.

[13] S.S. Sazhin, V.M. Gun'ko, R. Nasiri, Quantum-chemical analysis of the processes at the surfaces of Diesel fuel droplets, Fuel (2016) http://dx.doi.org/10.1016/j.fuel.2015.10.029 (in press).

[14] S.S. Sazhin, M. Al Qubeissi, R. Nasiri, V.M. Gunko, A.E. Elwardany, F. Lemoine, F., Grisch, M.R. Heikal, A multi-dimensional quasi-discrete model for the analysis of Diesel fuel droplet heating and evaporation, Fuel 129 (2004) 238-266.

[15] B. Abramzon, S.S. Sazhin, Convective vaporization of fuel droplets with thermal radiation absorption, Fuel 85 (2006) 32-46.

[16] F.P. Incropera, D.P. DeWitt, Fundamentals of Heat and Mass Transfer, Fifth Edition. New York, Chichester: John Wiley & Sons (2002).

[17] A.E. Elwardany, I.G. Gusev, G. Castanet, F. Lemoine, S.S. Sazhin, Mono- and multi-component droplet cooling/heating and evaporation: comparative analysis of numerical models, Atomization and Sprays 21 (2011), 907-931.

[18] S. Tonini, G.E. Cossali, An analytical model of liquid drop evaporation in gaseous environment. Int. J. Thermal Sciences 57 (2012) 45-53.

[19] S. Tonini, G.E. Cossali, A novel vaporisation model for a single-component drop in high temperature air streams. Int. J. Thermal Sciences 75 (2014) 194-203.

[20] S.S. Sazhin, I.N. Shishkova, M. Heikal, Kinetic modelling of fuel droplet heating and evaporation: calculations and approximations, Int. J. Engineering Systems Modelling and Simulation 2 (2010), 169-176.

Figure Captions

Fig. 1 Liquid, kinetic and hydrodynamic regions near the surface of the droplet. T_s is the droplet surface temperature, $\rho_{s\,(n,p)}$ are n-dodecane $(_n)$ and p-dipropylbenzene $(_p)$ vapour densities in the immediate vicin-

ity of the droplet surface, T_{Rd} and $\rho_{Rd\,(n,p)}$ are the temperature and n-dodecane ($_n$) and p-dipropylbenzene ($_p$) vapour densities at the outer boundary of the kinetic region.

Fig. 2 The plots of normalised mass fluxes $\tilde{j} \equiv j/(\rho_0\sqrt{R_v T_0})$ predicted by the kinetic (line 'k') and hydrodynamic (lines 'h') models for a stationary n-dodecane droplet versus $\alpha_\rho \equiv \rho_{Rd}/\rho_s$ (normalised vapour density at the outer boundary of the kinetic region). Droplet surface and gas temperatures are assumed equal to 600 K and 1000 K respectively. The values of α_ρ inferred from iteration 2 and higher iterations are indistinguishable.

Fig. 3 The plots of normalised heat fluxes $\tilde{q} \equiv q/(p_0\sqrt{R_v T_0})$ predicted by the kinetic (line 'k') and hydrodynamic (lines 'h') models for a stationary n-dodecane droplet versus $\alpha_T \equiv T_{Rd}/T_s$ (normalised temperature at the outer boundary of the kinetic region). Droplet surface and gas temperatures are assumed equal to 600 K and 1000 K respectively. The values of α_T inferred from iteration 2 and higher iterations are indistinguishable.

Fig. 4 The same as Fig. 2 but for a droplet moving with velocity 10 m/s. In this case there is a visible difference between the results inferred from iteration 2 and iteration 50.

Fig. 5 The same as Fig. 3 but for a droplet moving with velocity 10 m/s. In this case there is a visible difference between the results inferred from iteration 2 and iteration 50.

Fig. 6 The plots of α_ρ versus T_s for a stationary n-dodecane droplet immersed in gas (air) at temperature equal to 800 K. The values of α_ρ inferred from iteration 2 and higher iterations are indistinguishable.

Fig. 7 The plots of α_T versus T_s for a stationary n-dodecane droplet immersed in gas (air) at temperature equal to 800 K. The values of α_T inferred from iteration 2 and higher iterations are indistinguishable.

Fig. 8 The plots of α_ρ versus T_s for a stationary n-dodecane droplet immersed in gas (air) at temperature equal to 1000 K. The values of α_ρ inferred from iteration 2 and higher iterations are indistinguishable.

Fig. 9 The plots of α_T versus T_s for a stationary n-dodecane droplet immersed in gas (air) at temperature equal to 1000 K. The values of α_T inferred from iteration 2 and higher iterations are indistinguishable.

Fig. 10

The plots of α_ρ versus T_s for a n-dodecane droplet moving with velocity 10 m/s in gas (air) at temper-

ature equal to 1000 K.

Fig. 11 The plots of α_T versus T_s for a n-dodecane droplet moving with velocity 10 m/s in gas (air) at temperature equal to 1000 K.

Fig. 12 The plots of α_ρ versus T_s for a stationary n-dodecane droplet immersed in gas (air) at temperature equal to 1200 K. The values of α_ρ inferred from iteration 2 and higher iterations are indistinguishable.

Fig. 13 The plots of α_T versus T_s for a stationary n-dodecane droplet immersed in gas (air) at temperature equal to 1200 K. The values of α_T inferred from iteration 2 and higher iterations are indistinguishable.

Fig. 14 The plots of $\alpha_{\rho\, n} \equiv \rho_{Rd\,(n)}/\rho_{s\,(n)}$ (normalised n-dodecane density) versus T_s for a stationary bi-component droplet (a mixture of 80% n-dodecane and 20% p-dipropylbenzene) immersed in gas (air) at temperature equal to 1000 K. The values of α_ρ inferred from iteration 2 and higher iterations are indistinguishable.

Fig. 15 The plots of $\alpha_{\rho\, p} \equiv \rho_{Rd\,(p)}/\rho_{s\,(p)}$ (normalised p-dipropylbenzene density) versus T_s for a stationary bi-component droplet (a mixture of 80% n-dodecane and 20% p-dipropylbenzene) immersed in gas (air) at temperature equal to 1000 K. The values of α_ρ inferred from iteration 2 and higher iterations are indistinguishable.

Fig. 16 The plots of α_T versus T_s for a stationary bi-component droplet (a mixture of 80% n-dodecane and 20% p-dipropylbenzene) immersed in gas (air) at temperature equal to 1000 K. The values of α_ρ inferred from iteration 2 and higher iterations are indistinguishable.

Fig. 17 The plots of $\alpha_{\rho\, n} \equiv \rho_{Rd\,(n)}/\rho_{s\,(n)}$ (normalised n-dodecane density) versus T_s for a bi-component droplet (a mixture of 80% n-dodecane and 20% p-dipropylbenzene) moving with velocity 10 m/s in gas (air) at temperature equal to 1000 K.

Fig. 18 The plots of $\alpha_{\rho\, p} \equiv \rho_{Rd\,(p)}/\rho_{s\,(p)}$ (normalised p-dipropylbenzene density) versus T_s for a bi-component droplet (a mixture of 80% n-dodecane and 20% p-dipropylbenzene) moving with velocity 10 m/s in gas (air) at temperature equal to 1000 K.

Fig. 19 The plots of α_T versus T_s for a bi-component droplet (a mixture of 80% n-dodecane and 20% p-dipropylbenzene) moving with velocity 10 m/s in gas (air) at temperature equal to 1000 K.

Fig. 20 The plots of R_d and T_s versus time, as predicted by the kinetic (solid) and hydrodynamic (dashed) models for a stationary n-dodecane droplet with initial radius and temperature equal to 5 μm and 300 K, respectively, immersed in a gas (air) at temperature 1000 K.

Fig. 21 The same as Fig. 20, but for a stationary bi-component droplet (a mixture of 80% n-dodecane and 20% p-dipropylbenzene).

Fig. 22 The same as Fig. 21, but for a droplet moving with velocity 10 m/s.

Fig. 23 The same as Fig. 22, but for mass fractions of n-dodecane (Y_n) and p-dipropylbenzene (Y_p) at the surface of the droplet.

Appendix 1

Approximations of α_ρ, $\alpha_{\rho\, n}$, $\alpha_{\rho\, p}$ and α_T versus T_s (iteration 50)

All approximations have been obtained for temperatures T_s in the range 300-650 K.

Figs. (6) and (7) ($T_g = 800$ K, a stationary n-dodecane droplet):

$$\alpha_\rho = 0.95127 + 6.62107\,10^{-4}\,T_s - 3.55461\,10^{-6}\,T_s^2 + 9.36931\,10^{-9}\,T_s^3 - 1.2005\,10^{-11}\,T_s^4$$

$$+5.87685\,10^{-15}\,T_s^5,$$

$$\alpha_T = 2.16074 - 0.01843\,T_s + 1.24389\,10^{-4}\,T_s^2 - 4.59688\,10^{-7}\,T_s^3 + 1.00627\,10^{-9}\,T_s^4$$

$$-1.30565\,10^{-12}\,T_s^5 + 9.29602\,10^{-16}\,T_s^6 - 2.80028\,10^{-19}\,T_s^7.$$

Figs. (8) and (9) ($T_g = 1000$ K, a stationary n-dodecane droplet):

$$\alpha_\rho = 0.97924 + 3.38661\,10^{-4}\,T_s - 2.10013\,10^{-6}\,T_s^2 + 6.19675\,10^{-9}\,T_s^3 - 0.864558\,10^{-11}\,T_s^4$$

$$+4.47852\,10^{-15}\,T_s^5,$$

$$\alpha_T = 3.09685 - 0.03312\,T_s + 2.22137\,10^{-4}\,T_s^2 - 8.15444\,10^{-7}\,T_s^3 + 1.77164\,10^{-9}\,T_s^4$$

$$-2.27837\,10^{-12}\,T_s^5 + 16.049\,10^{-16}\,T_s^6 - 4.77199\,10^{-19}\,T_s^7.$$

Figs. (10) and (11) ($T_g = 1000$ K, an n-dodecane droplet moving with relative velocity 10 m/s):

$$\alpha_\rho = 1.37063 - 0.00428\,T_s + 1.88185\,10^{-5}\,T_s^2 - 3.89817\,10^{-8}\,T_s^3 + 3.7469\,10^{-11}\,T_s^4$$

$$-1.34491\,10^{-14}\,T_s^5,$$

$$\alpha_T = 4.74618 - 0.05942\,T_s + 4.02544\,10^{-4}\,T_s^2 - 1.49552\,10^{-6}\,T_s^3 + 3.2968\,10^{-9}\,T_s^4$$

$$-4.31537\,10^{-12}\,T_s^5 + 3.1035\,10^{-15}\,T_s^6 - 9.44769\,10^{-19}\,T_s^7.$$

Figs. (12) and (13) ($T_g = 1200$ K, a stationary n-dodecane droplet):

$$\alpha_\rho = 1.02633 - 2.13871\,10^{-4}\,T_s + 4.31389\,10^{-7}\,T_s^2 + 5.43478\,10^{-10}\,T_s^3 - 2.48699\,10^{-12}\,T_s^4$$

$$+1.84009\,10^{-15}\,T_s^5,$$

$$\alpha_T = 3.60953 - 0.04105\,T_s + 2.74138\,10^{-4}\,T_s^2 - 1.00118\,10^{-6}\,T_s^3 + 2.16179\,10^{-9}\,T_s^4$$

$$-2.75897\ 10^{-12}\,T_s^5 + 1.92458\ 10^{-15}\,T_s^6 - 5.65003\ 10^{-19}\,T_s^7.$$

Figs. (14), (15) and (16) ($T_g = 1000$ K, a stationary bi-component (a mixture of 80% n-dodecane and 20% p-dipropylbenzene) droplet):

$$\alpha_{\rho\,n} = 0.84400 + 0.00193\,T_s - 9.46424\ 10^{-6}\,T_s^2 + 2.29404\ 10^{-8}\,T_s^3 - 2.736\ 10^{-11}\,T_s^4$$

$$+1.27255\ 10^{-14}\ T_s^5,$$

$$\alpha_{\rho\,p} = 0.95587 + 5.37126\ 10^{-4}\,T_s - 2.58165\ 10^{-6}\,T_s^2 + 6.11316\ 10^{-9}\,T_s^3 - 7.10412\ 10^{-12}\,T_s^4$$

$$+3.21354\ 10^{-15}\ T_s^5,$$

$$\alpha_T = 2.62683 - 0.0219\,T_s + 1.21723\ 10^{-4}\,T_s^2 - 3.55272\ 10^{-7}\,T_s^3 + 5.75889\ 10^{-10}\,T_s^4$$

$$-4.92827\ 10^{-13}\,T_s^5 + 1.74267\ 10^{-16}\,T_s^6.$$

Figs. (17), (18) and (19) ($T_g = 1000$ K, a bi-component (a mixture of 80% n-dodecane and 20% p-dipropylbenzene) droplet moving with relative velocity 10 m/s):

$$\alpha_{\rho\,n} = 0.96092 + 6.31887\ 10^{-4}\,T_s - 4.26513\ 10^{-6}\,T_s^2 + 1.42574\ 10^{-8}\,T_s^3 - 2.27105\ 10^{-11}\,T_s^4$$

$$+1.3282\ 10^{-14}\ T_s^5,$$

$$\alpha_{\rho\,p} = 0.93763 + 7.74252\ 10^{-4}\,T_s - 3.86981\ 10^{-6}\,T_s^2 + 9.71485\ 10^{-9}\,T_s^3 - 1.21398\ 10^{-11}\,T_s^4$$

$$+5.90554\ 10^{-15}\ T_s^5,$$

$$\alpha_T = 5.8157 - 0.06441\,T_s + 3.55615\ 10^{-4}\,T_s^2 - 1.02948\ 10^{-6}\,T_s^3 + 1.65178\ 10^{-9}\,T_s^4$$

$$-1.39642\ 10^{-12}\,T_s^5 + 4.86933\ 10^{-16}\,T_s^6.$$

The accuracy of these approximations for α_ρ and α_T for stationary n-dodecane droplets immersed in gas (air) at temperature 1000 K is illustrated in Figs. A1 and A2. The accuracy of the same approximations but for a droplet moving with relative velocity 10 m/s is illustrated in Figs. A3 and A4.

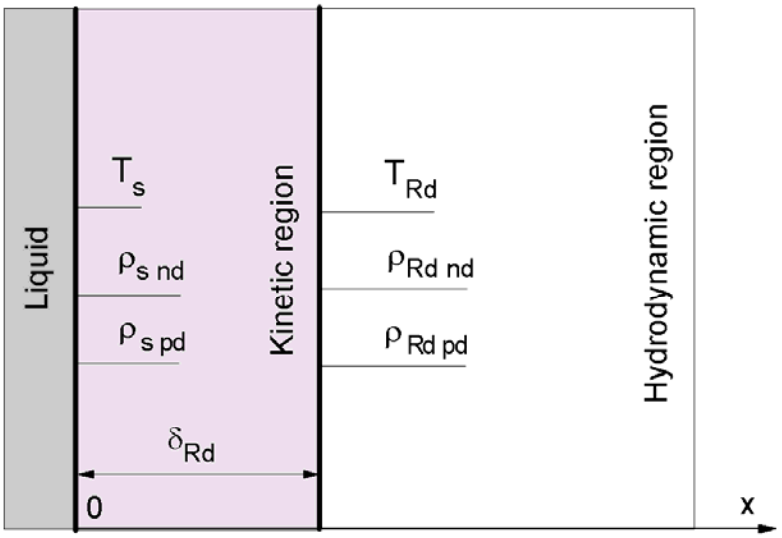
Liquid
T_s
$\rho_{s\,nd}$
$\rho_{s\,pd}$
Kinetic region
T_{Rd}
$\rho_{Rd\,nd}$
$\rho_{Rd\,pd}$
Hydrodynamic region
δ_{Rd}
0
x

Fig.1.

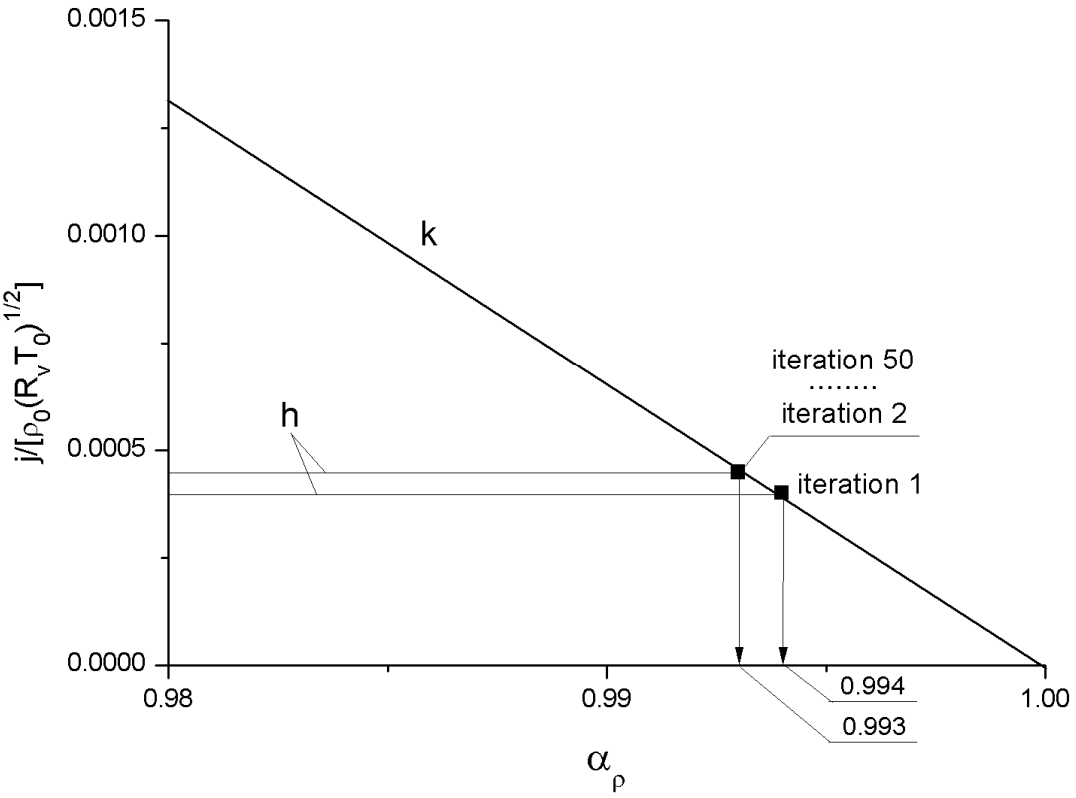
0.0015
0.0010
0.0005
0.0000
k
h
iteration 50
iteration 2
iteration 1
0.994
0.993
0.98
0.99
1.00
$j/[\rho_0(R_vT_0)^{1/2}]$
α_ρ

Fig.2.

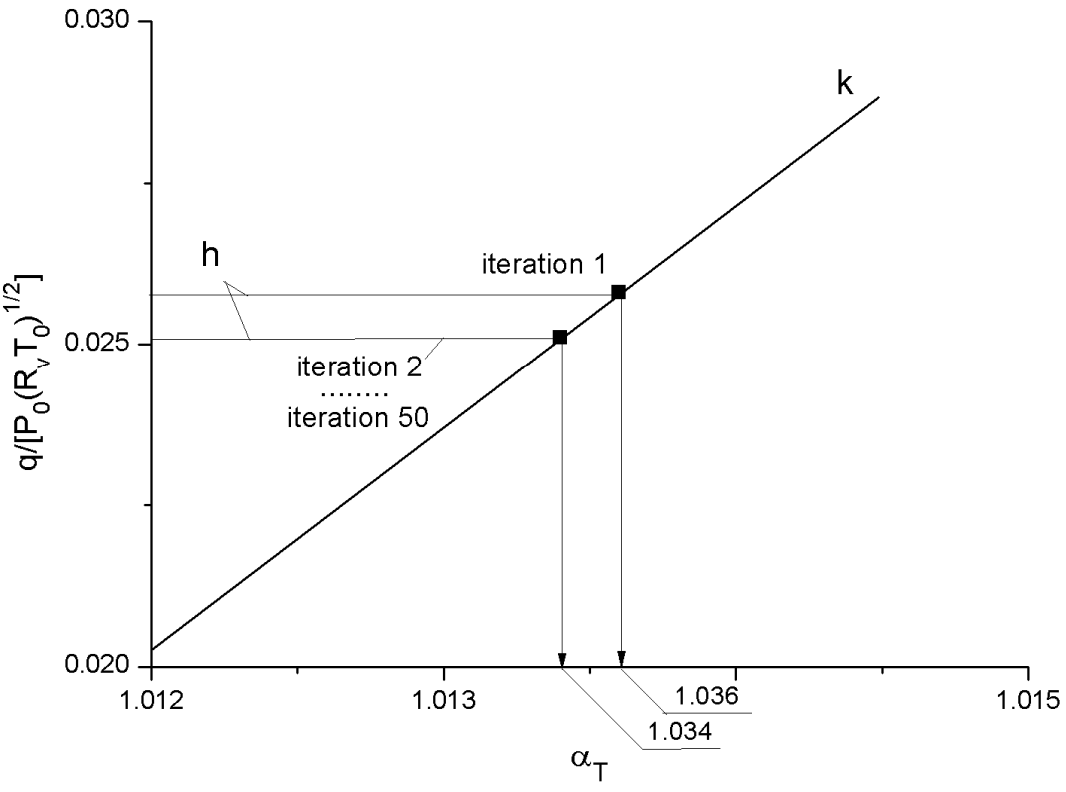
0.030
0.025
0.020
k
h
iteration 1
iteration 2
iteration 50
1.036
1.034
1.012
1.013
1.015
$q/[P_0(R_vT_0)^{1/2}]$
α_T

Fig.3.

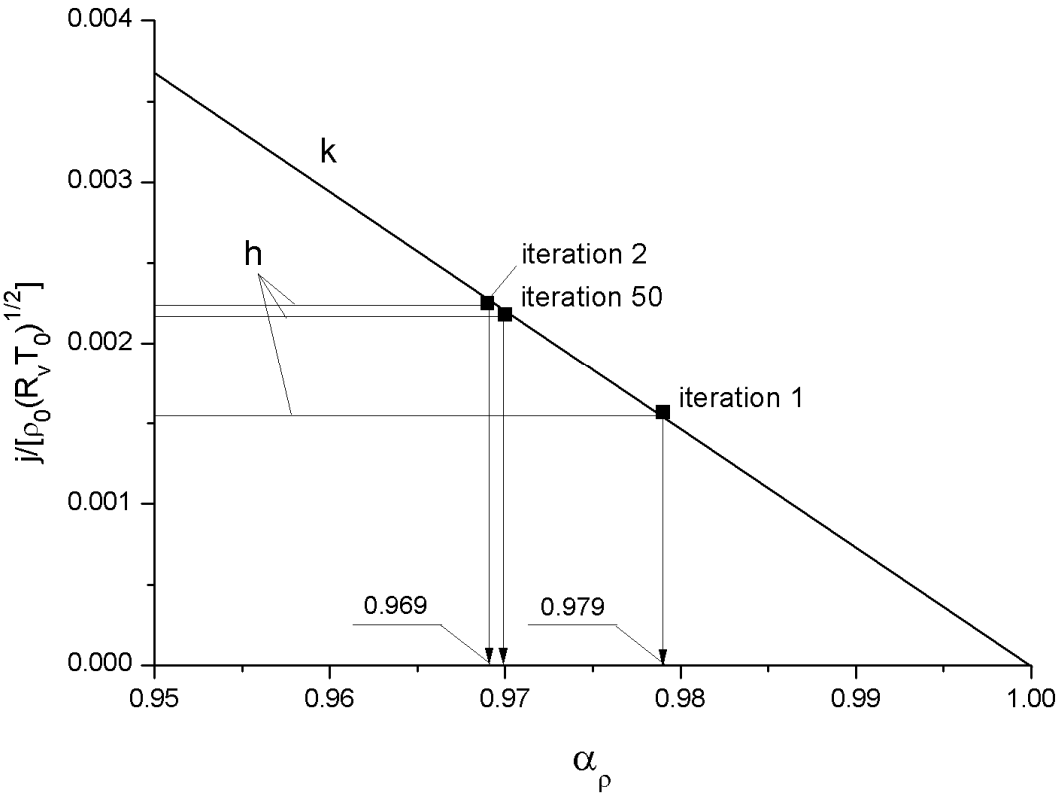
0.004
0.003
0.002
0.001
0.000
0.95
0.96
0.97
0.98
0.99
1.00
k
h
iteration 2
iteration 50
iteration 1
0.969
0.979
$j/[\rho_0(R_v T_0)^{1/2}]$
α_ρ

Fig.4.

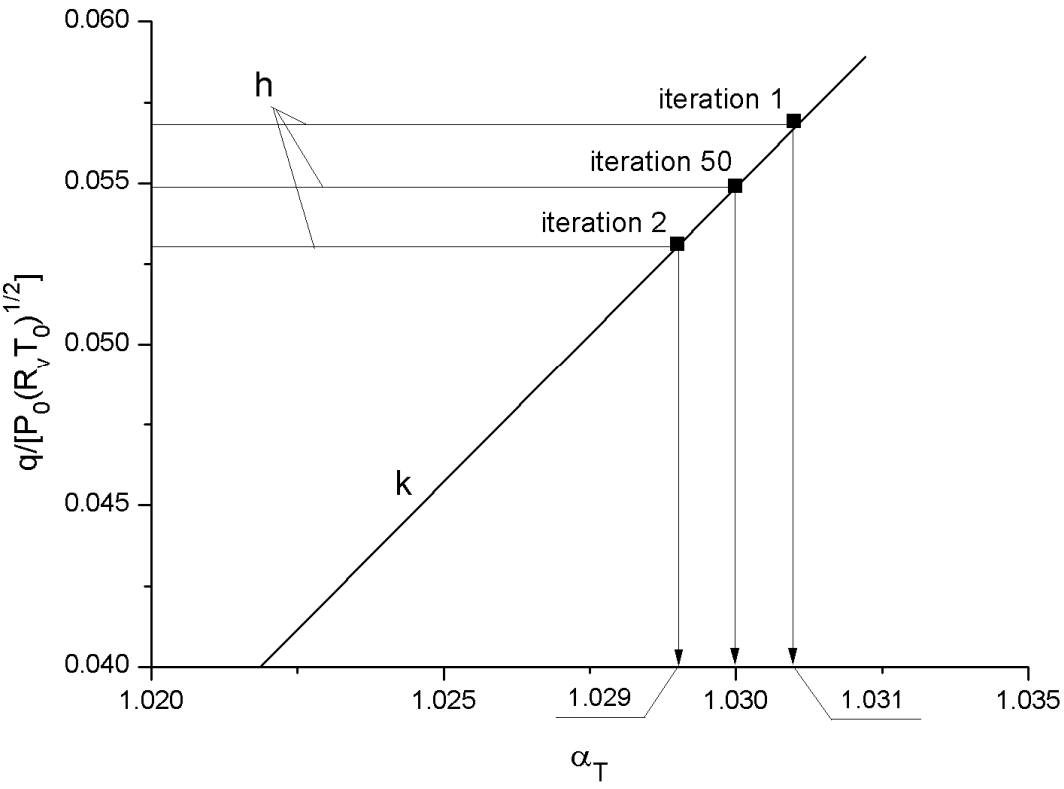
0.060
0.055
0.050
0.045
0.040
1.020
1.025
1.029
1.030
1.031
1.035
h
iteration 1
iteration 50
iteration 2
k
$q/[P_0(R_v T_0)^{1/2}]$
α_T

Fig.5.

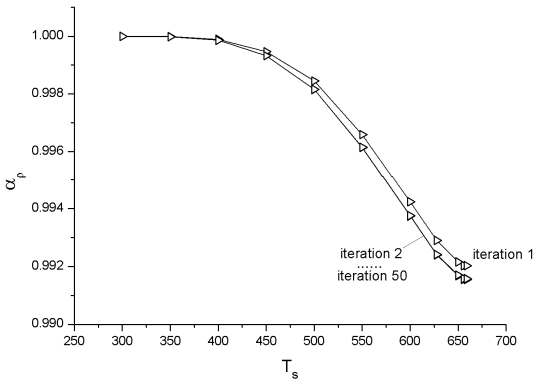

Fig.6.

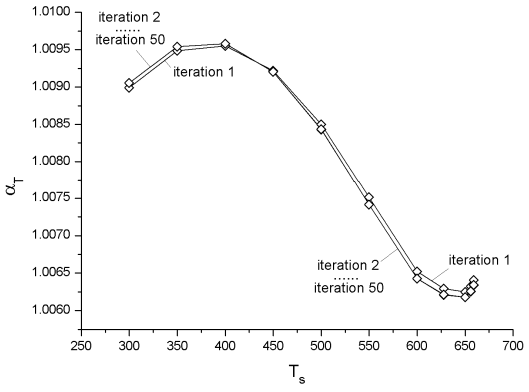

Fig.7.

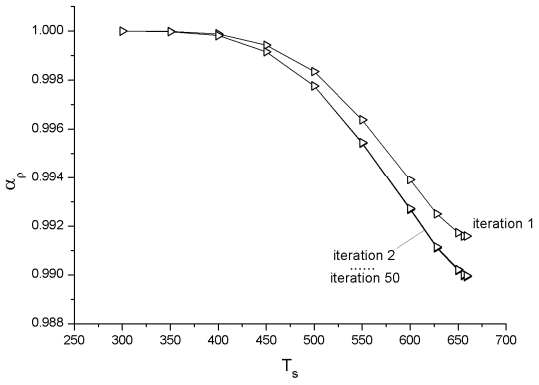

Fig.8.

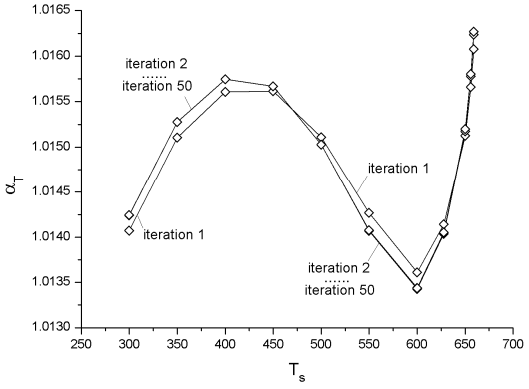

Fig.9.

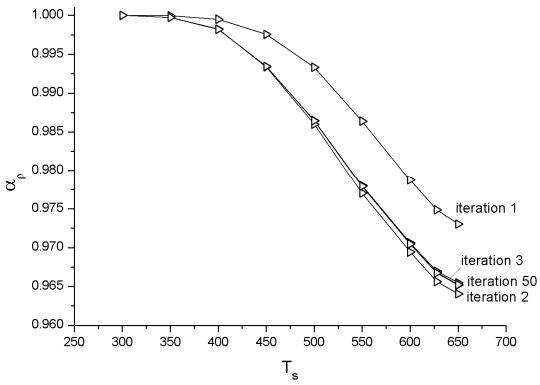

Fig.10.

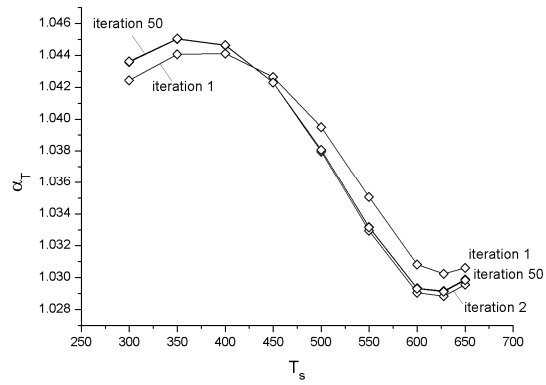

Fig.11.

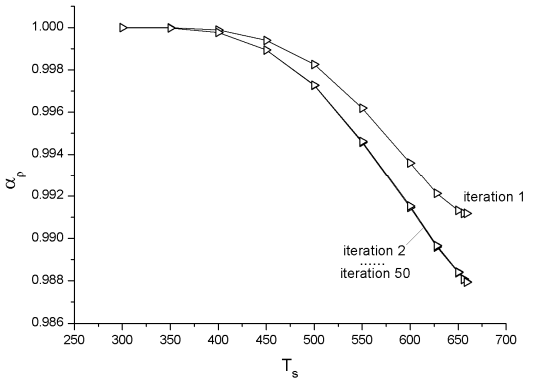

Fig.12.

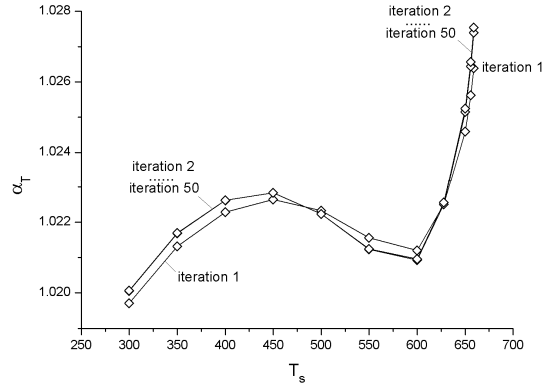

Fig.13.

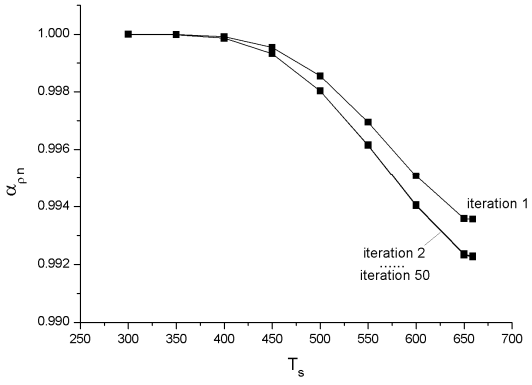

Fig.14.

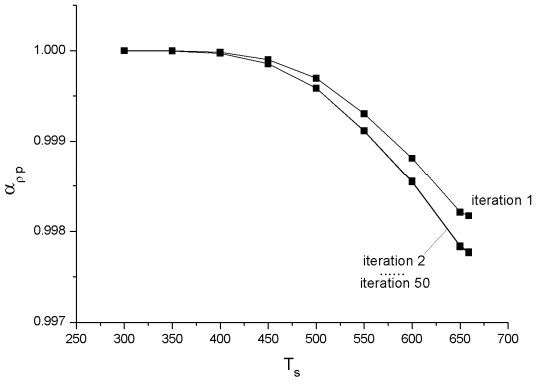

Fig.15.

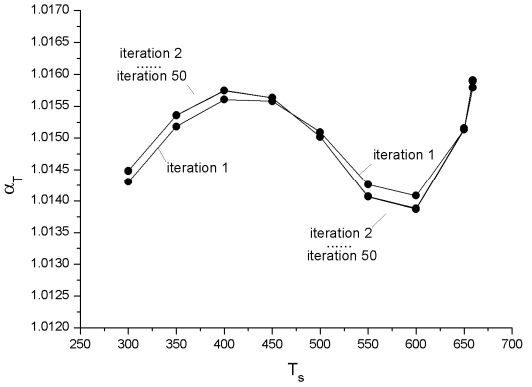

Fig.16.

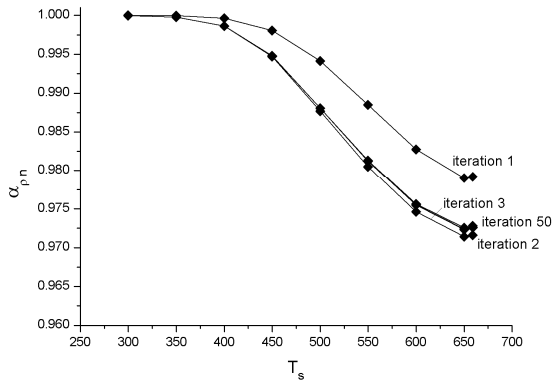

Fig.17.

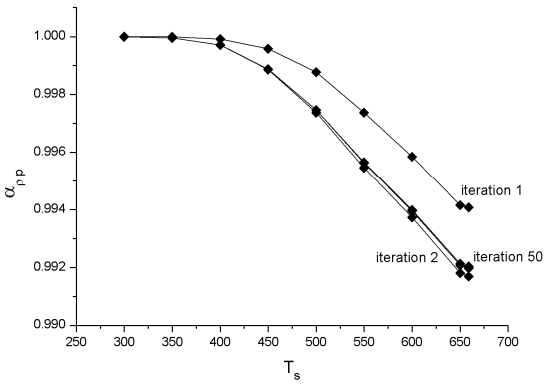

Fig.18.

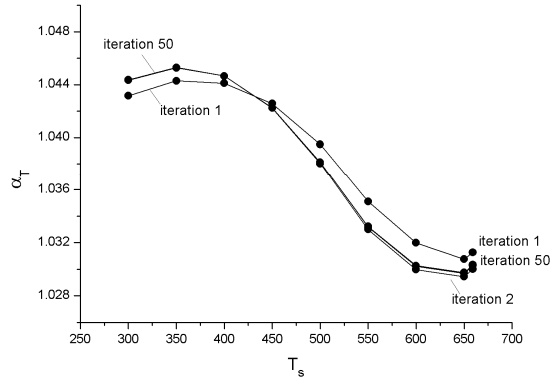

Fig.19.

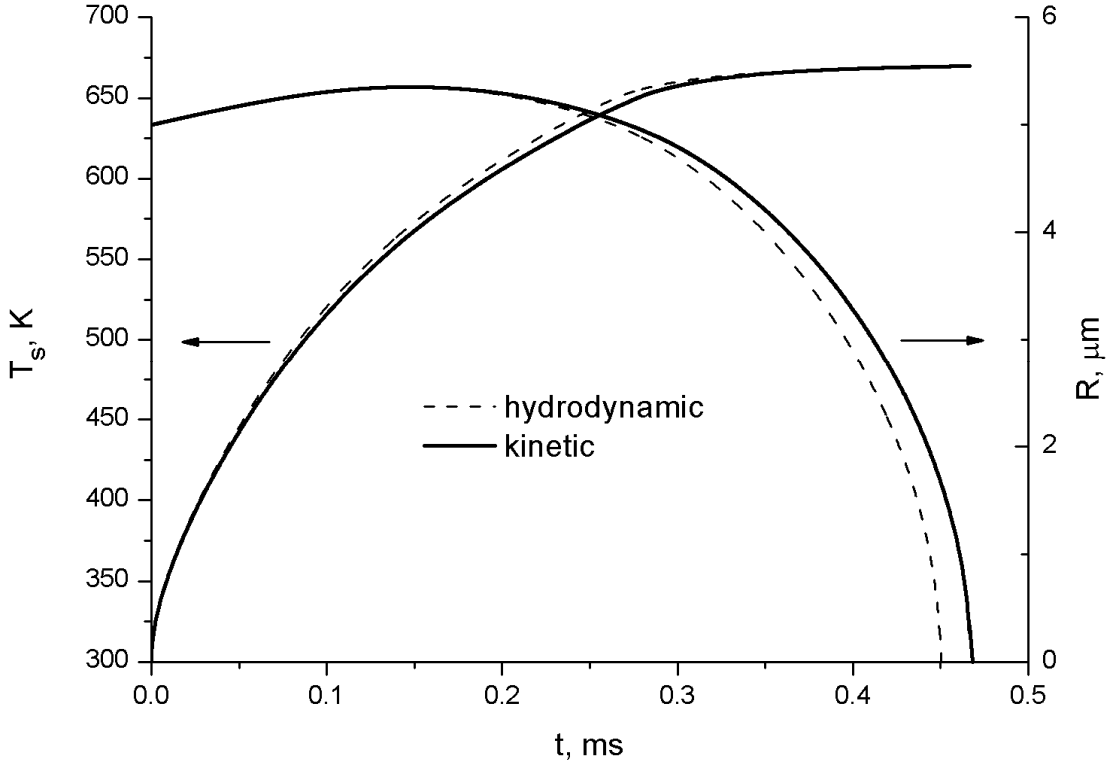
700
650
600
550
500
450
400
350
300
T_s, K
6
4
2
0
R, μm
0.0
0.1
0.2
0.3
0.4
0.5
t, ms
hydrodynamic
kinetic

Fig.20.

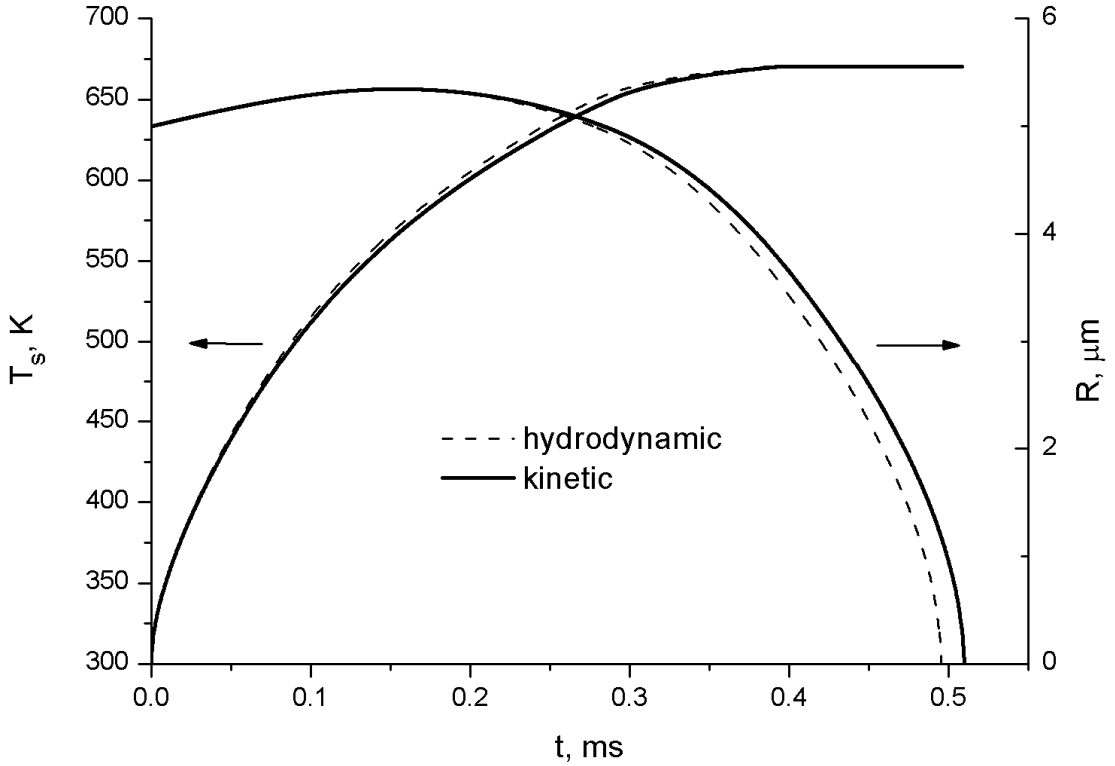
700
650
600
550
500
450
400
350
300
T_s, K
6
4
2
0
R, μm
0.0
0.1
0.2
0.3
0.4
0.5
t, ms
hydrodynamic
kinetic

Fig.21.

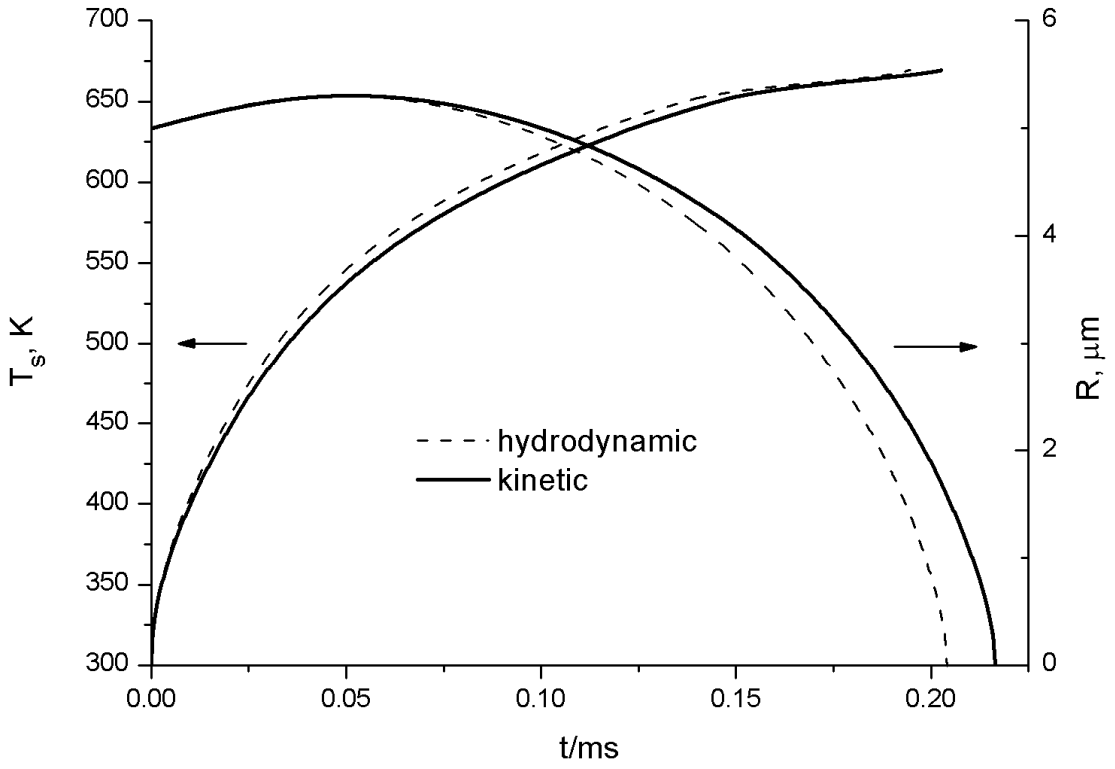
700
650
600
550
500
450
400
350
300
T_s, K
6
4
2
0
R, μm
0.00
0.05
0.10
0.15
0.20
t/ms
hydrodynamic
kinetic

Fig.22.

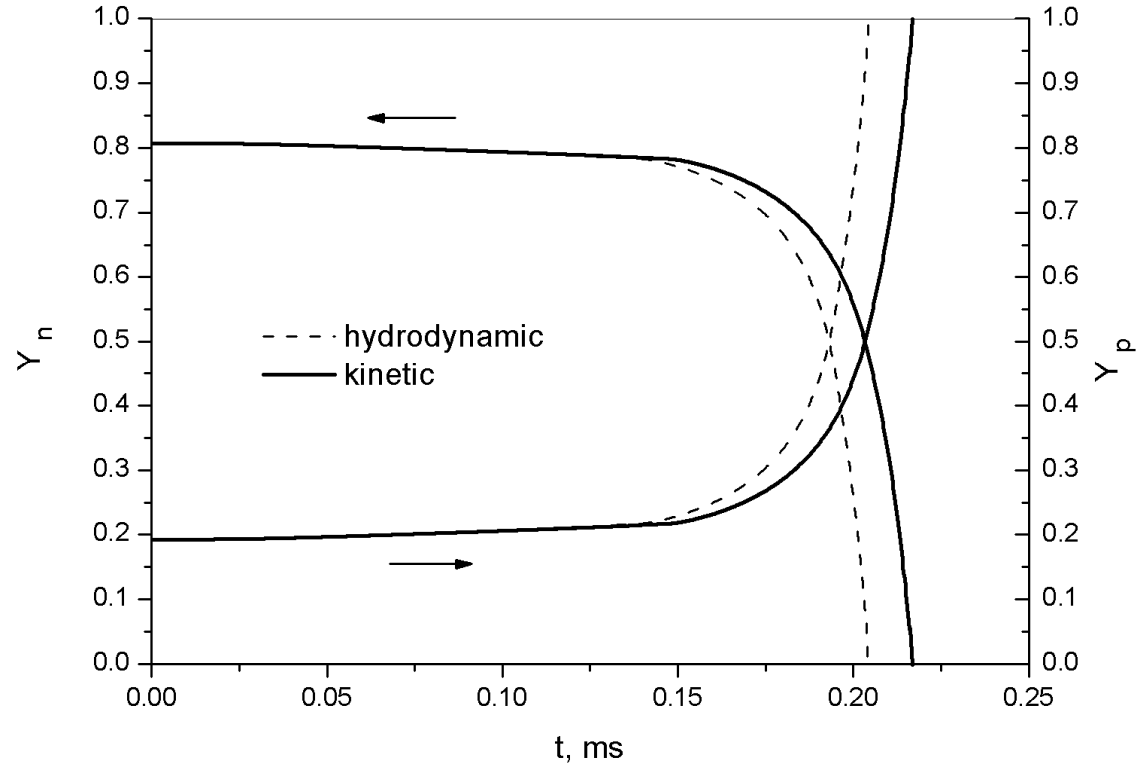
1.0
0.9
0.8
0.7
0.6
0.5
0.4
0.3
0.2
0.1
0.0
Y_n
Y_p
0.00
0.05
0.10
0.15
0.20
0.25
t, ms
hydrodynamic
kinetic

Fig.23.

Appendix

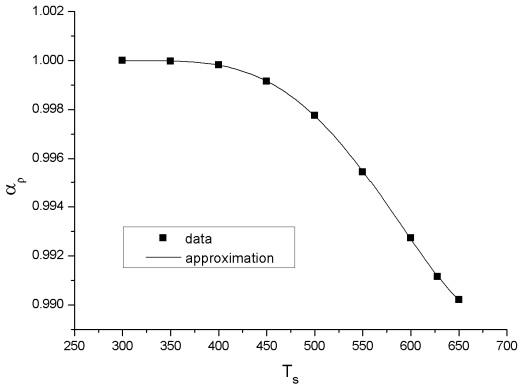

Fig.A1.

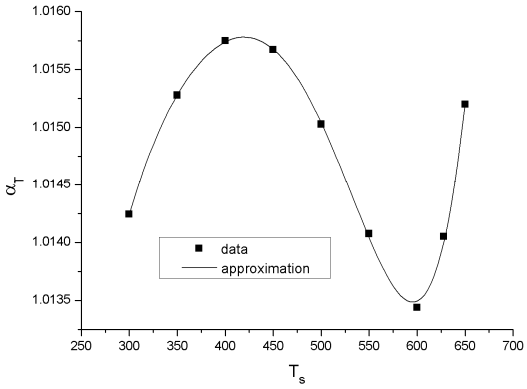

Fig.A2.

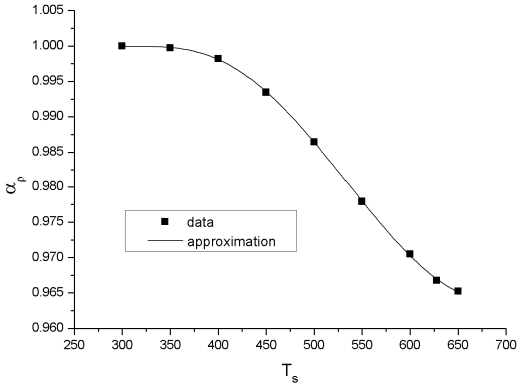

Fig.A3.

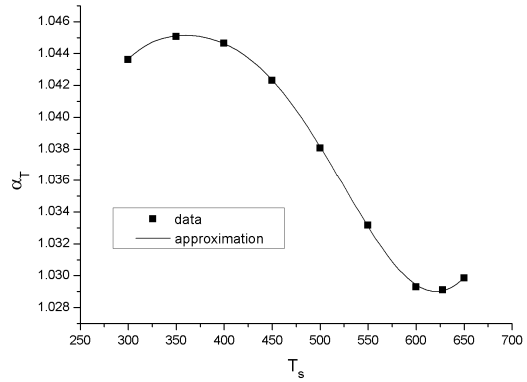

Fig.A4.